Among these are ease of synthesis and purification, high stability toward air and moisture, and their ability to generate microcrystalline SnS and SnSe powders cleanly and conveniently by simple heating to 450 °C under a helium atmosphere.

Acknowledgment. Financial support from the Air Force Office of Scientific Research through Grants 88-0060 and 91-0197 and Dow Corning Corp. is gratefully acknowledged. We also thank Jody Solem and Jason Bender for their help in aquiring XRD patterns and Dr. Thomas Freeman for obtaining SEM photographs.

Registry No. 1, 15287-09-9; 2, 132776-76-2; 3, 16892-66-3; 4, 105860-17-1; Ph_2SnCl_2, 1135-99-5; Ph_2SiCl_2, 80-10-4; SnS, 1314-95-0; Ph_4Sn, 595-90-4; Ph_2S, 139-66-2; SnSe, 1315-06-6; Ph_2Se, 1132-39-4; $Ph_3SnSePh$, 29328-48-1.

Preparation, Ionic Conductivity, and Humidity-Sensing Property of Novel, Crystalline Microporous Germanates, $Na_3HGe_7O_{16}\cdot xH_2O$, x = 0–6. 1

Shouhua Feng, Menting Tsai, and Martha Greenblatt*

Department of Chemistry, Rutgers, The State University of New Jersey, New Brunswick, New Jersey 08903

Received September 23, 1991. Revised Manuscript Received December 3, 1991

A crystalline microporous germanate, $Na_3HGe_7O_{16}\cdot 6H_2O$, has been hydrothermally synthesized from a Na_2O–GeO_2–H_2O system. This phase undergoes a phase transition to $Na_3HGe_7O_{16}\cdot xH_2O$, x = 0–4 at ~160 °C. Both phases of the sodium germanates have been characterized by powder X-ray diffraction and differential thermal and thermogravimetric analyses. Sodium and proton ionic conductivities in $Na_3HGe_7O_{16}\cdot 6H_2O$, $Na_3HGe_7O_{16}\cdot 4H_2O$, and dehydrated $Na_3HGe_7O_{16}$ were studied by an ac impedance technique. In $Na_3HGe_7O_{16}\cdot 6H_2O$ motion of surface, bulk proton, and Na^+ ion respectively dominate the conductivity in different temperature ranges. The conductivity in dehydrated $Na_3HGe_7O_{16}$ is $\sim 10^{-8}$ $(\Omega\ cm)^{-1}$ at 125 °C and $\sim 10^{-3}$ $(\Omega\ cm)^{-1}$ at 500 °C with an activation energy E_a = 0.64 eV. Humidity-sensing property of $Na_3HGe_7O_{16}\cdot 6H_2O$ and $Na_3HGe_7O_{16}\cdot 4H_2O$ was investigated in the temperature range 50–120 °C.

Introduction

Since the 1950s many investigations of ionic conductivity of crystalline microporous aluminosilicate zeolites have been reported.[1-3] Less information is available on the ionic conductivity of the crystalline microporous germanates, $M_3HGe_7O_{16}\cdot 4$–$6H_2O$, M = Li^+, Na^+, K^+, NH_4^+, Rb^+, and Cs^+. Studies on the X-ray characterization,[4-8] NMR measurements,[9-11] and adsorption properties[12] have been published for germanates and some features of the structure have been determined based on powder X-ray diffraction (PXD) data.[13] The cubic framework structure of the germanates, which is identical to that of the mineral pharmacosiderite,[14] is built up of face- and edge-sharing GeO_6 octahedra which corner share with GeO_4 tetrahedra (Figure 1). In this structure, channels of eight-membered rings with a window size of 4.3 Å lie in the (100) directions connecting cavities in which mobile sodium cations and water molecules are located. This mixed tetrahedral–octahedral framework structure is novel and different from the traditional aluminosilicate zeolites where only TO_4 tetrahedra (T = Si, Al, or Ge) are the basic building units. Mixed TO_6 and TO_4 units are also found in the structures of recently synthesized microporous stannosilicates[15] and gallophosphates.[16,17]

In this paper we report the results of the ionic conductivity and humidity sensing property of the microporous Na–germanates.

Experimental Section

$Na_3HGe_7O_{16}\cdot 6H_2O$ was synthesized under hydrothermal conditions at 150–180 °C in sealed systems containing an aqueous mixture of sodium hydroxide and the α-quartz form of germanium dioxide. A typical synthetic procedure began with the combination of GeO_2 (Eagle-Picher Co., reagent grade) and the aqueous solution of NaOH (Fisher, reagent grade) to form an aqueous gel having molar composition $1.0Na_2O\cdot GeO_2\cdot 80H_2O$. Crystallization of the aqueous gel was carried out in stainless steel autoclaves lined with poly(tetrafluoroethylene) (PTFE) under autogenous pressure at 180 °C for 3 days. The crystalline product ($Na_3HGe_7O_{16}\cdot 6H_2O$) was filtered, washed with

* To whom correspondence should be addressed.

(1) Breck, D. W. *Zeolite Molecular Sieves, Synthesis, Structure and Use*; Wiley: New York, 1974; p 457.
(2) Andersen, E. K.; Andersen, I. G. K.; Skou, E.; Yde-Andersen, S. *Solid State Ionics* **1986**, *18* and *19*, 1170.
(3) Ozin, G. A.; Kuperman, A.; Stein, A. *Angew. Chem., Int. Ed. Engl.* **1989**, *3*, 28.
(4) Zemann, V. J. *Acta Crystallogr.* **1959**, *12*, 252.
(5) Bittner, H.; Kerber, W. *Monatsh. Chem.* **1969**, *100*, 427.
(6) Hauser, E.; Nowotny, H.; Seifert, K. J. *Monatsh. Chem.* **1970**, *101*, 715.
(7) Hauser, E.; Bittner, H.; Nowotny, H. *Monatsh. Chem.* **1970**, *101*, 1864.
(8) Seifert, K. J.; Nowotny, H.; Hauser, E. *Monatsh. Chem.* **1971**, *102*, 1006.
(9) Wada. T.; Cohen-Addad, J. P. *Bull. Soc. Fr. Mineral. Cristallogr.* **1969**, *92*(2), 238.
(10) Bittner, H.; Hauser, E. *Monatsh. Chem.* **1970**, *101*, 1471.
(11) Hauser, E.; Hoch, M. J. R. *J. Magn. Reson.* **1973**, *10*, 211.
(12) Nowotny, H.; Wittmann, A. *Monatsh. Chem.* **1954**, *85*, 558.
(13) Wittmann, A. *Fortschr. Miner.* **1966**, *43*(2), 230.
(14) Wilson, A. J. C., Ed. *Structure Reports*; Oosthoek-Utrecht: The Netherlands, 1947–1948; Vol. 11, p 405.
(15) Corcoran, E. W.; Nawsam, Jr. J. M.; King, Jr. H. E. and Vaughan, D. E. W. *Zeolite Synthesis*; Occelli, M., Robson, H. E., Eds.; 1989; p 603.
(16) Feng, S.; Xu, R.; Yang, G.; Shun, H. *Chem. J. Chinese Univ. (Engl. Ed.)* **1988**, *4* (2), 9.
(17) Wang, T.; Yang, G.; Feng, S.; Shang, C.; Xu, R. *J. Chem. Soc., Chem. Commun.* **1989**, *2436*.

0897-4756/92/2804-0388$03.00/0

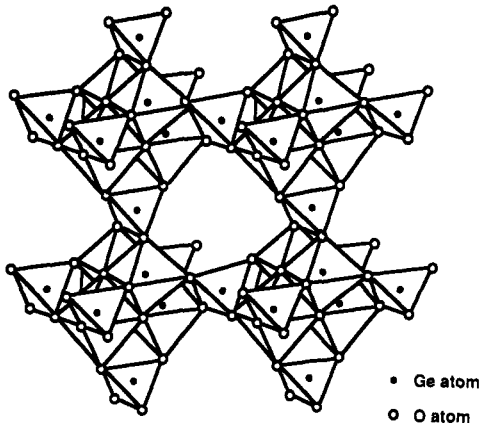

Figure 1. Framework structure of Na–germanate showing the linking of GeO_4 tetrahedra and GeO_6 octahedra.

distilled water, dried at ambient temperature, and then identified by powder X-ray diffraction analysis. $Na_3HGe_7O_{16}{\cdot}xH_2O$ (x = 0–4) was prepared by heating $Na_3HGe_7O_{16}{\cdot}6H_2O$ at 200 °C for 2 h.

The PXD patterns were recorded on a Scintag X-ray diffractometer using monochromized Cu Kα radiation. A high-temperature X-ray diffraction system was used to investigate the phase transition. Unit cell parameters were obtained by using a least-squares method. Silicon was used as an internal standard.

Differential thermal and thermogravimetric analysis (DTA and TGA) were carried out on a Du Pont Model 9900 thermal analyzer with a heating rate of 4 °C/min in air.

FTIR spectra were recorded at room temperature on a Perkin-Elmer infrared Fourier transform spectrometer (Model 1720) on samples in KBr pellets at room temperature in the range 400–4000 cm^{-1} with 2-cm^{-1} resolution. Prior to the measurement, the dehydrated sample was heat treated at 400 °C under vacuum ($\sim 10^{-2}$ Torr).

For the ionic conductivity measurement the samples were pelletized under 10^2 lb/in.^{2}. Ionic conductivities were measured in air, flowing dried Ar, and vacuum by ac impedance technique using a Solartron Model 1250 frequency analyzer and 1186 electrochemical interface that were equipped with a Hewlett-Packard 9816 desk-top computer for data collection and analysis. Electrode connection to disk-shaped samples was made by coating the faces of the pellets with platinum ink. A frequency range of 10 Hz to 65 kHz (100 Hz to 65 KHz for certain cases) and a heating rate of 2 °C/min were used throughout.

The measurement of humidity sensing was carried out in a Fisher Scientific Model 282A Isotemp vacuum oven with the temperature control at ±1 °C. The partial pressures of water (P_{H_2O}) were controlled by injecting calculated amounts of water into the oven which was pumped to 10^{-2} Torr prior to the humidity-sensing measurements.

Results and Discussion

Synthesis. $Na_3HGe_7O_{16}{\cdot}6H_2O$ can be simply crystallized from the starting mixtures with molar composition range (1.0–1.5)$Na_2O{\cdot}GeO_2{\cdot}$(50–150)H_2O at 150–180 °C. The content of NaOH determines the nature and the yields of desired products. From the synthetic reactions

$$2NaOH + GeO_2 \rightarrow Na_2GeO_3 + H_2O \quad (1)$$

$$7Na_2GeO_3 + 12H_2O \rightarrow Na_3HGe_7O_{16}{\cdot}6H_2O + 11NaOH \quad (2)$$

it is known that excess NaOH ($Na_2O/GeO_2 > 1.5$) leads to the dissolution of the product Na–germanate, whereas composition deficient in NaOH ($Na_2O/GeO_2 < 1.0$) results in unreacted GeO_2. Thus optimal NaOH content is necessary to obtain a pure product and good yield. Under the experimental conditions, the product $Na_3HGe_7O_{16}{\cdot}6H_2O$ is obtained as a pure single phase with high crystallinity.

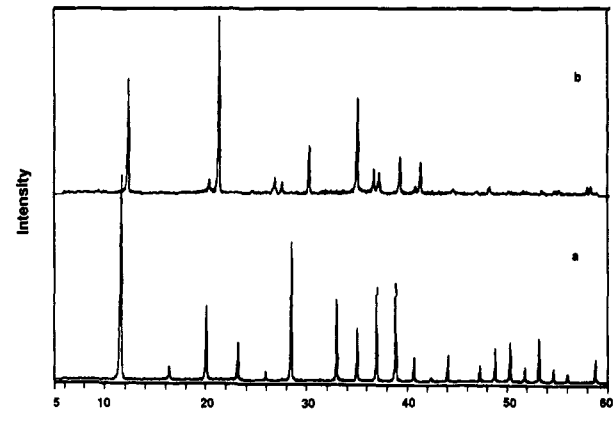

Figure 2. Powder X-ray diffraction patterns of Na–germanates; (a) phase I and (b) phase II.

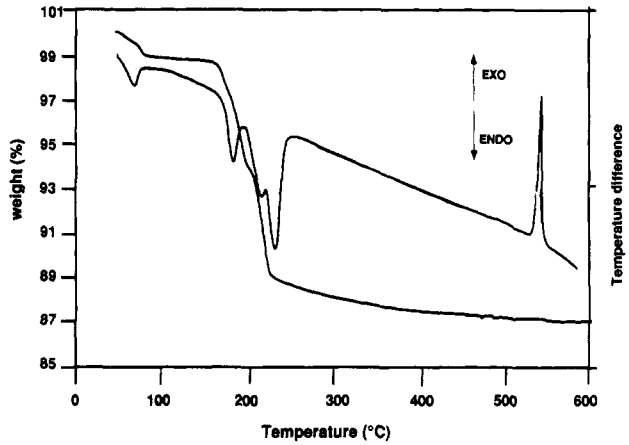

Figure 3. DTA-TG curves of $Na_3HGe_7O_{16}{\cdot}6H_2O$; the transition temperature to $Na_3HGe_7O_{16}{\cdot}4H_2O$ is at 160 °C.

Characterization. (1) PXD. Figure 2 shows the PXD patterns of $Na_3HGe_7O_{16}{\cdot}6H_2O$ (phase I) and $Na_3HGe_7O_{16}{\cdot}4H_2O$ (phase II) at 25 °C respectively. The unit cell parameter of $Na_3HGe_7O_{16}{\cdot}6H_2O$ is a = 7.72 (3) Å as determined by least-squares analysis of the observed PXD data (Figure 2a) according to the proposed space group $P\bar{4}3m$.[4] The structure of $Na_3HGe_7O_{16}{\cdot}xH_2O$ (x = 0–4) formed at 160 °C is quite different as shown in Figure 2b. The shift to higher degree (2θ) of the first diffraction peak indicates a decrease of the unit cell parameter. This is probably due to the loss of water molecules that serve as structure templates. The results of high-temperature powder X-ray diffraction indicate that the structure changes continuously with increasing temperature from about 160 to 200 °C, even though the DTA suggest three first-order phase transitions between 160 and 200 °C.

(2) DTA-TGA. DTA-TGA curves (Figure 3) indicate that $Na_3HGe_7O_{16}{\cdot}6H_2O$ first loses weight (~1%) from 20 to 50 °C; a weak endothermic peak is also seen in the DTA at ~60 °C. This anomaly is ascribed to loss of surface water. This process is reversible, and a weight gain of the same sample is observed in the TGA upon cycling in air between room temperature and 120 °C (Figure 4). The onset of continuous weight loss at ~160 to ~450 °C in the TGA and three sharp endotherms in the DTA at

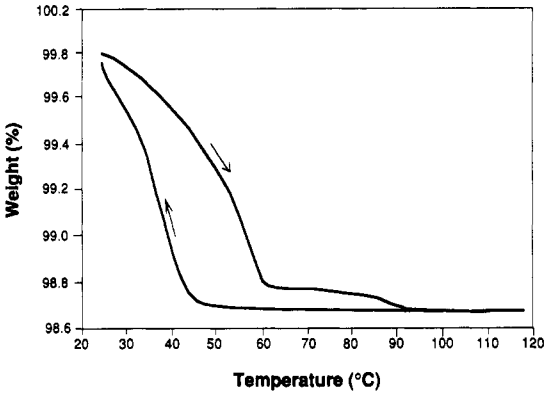

Figure 4. TG curve of $Na_3HGe_7O_{16}{\cdot}6H_2O$ showing surface water readsorption, humidity is ~60%.

~160–210 °C are associated with the gradual loss of 6 H_2O from $Na_3HG_7O_{16}{\cdot}6H_2O$. The PXD of the sample heated in the DTA/TGA to just above ~160 °C indicates a structural phase transition (Figure 2b). The water loss (~2 H_2O) leading to this transition is irreversible (i.e., the sample cannot be rehydrated by exposing it to the ambient or by equilibration in saturated water vapor). The two strong endothermic peaks at 187 and 212 °C (Figure 3) correspond to further loss of H_2O in $Na_3HGe_7O_{16}{\cdot}xH_2O$ (x = 4–0, phase II). The TGA shows a total water loss of 11.6% (Figure 3) from 50 to 450 °C consistent with the theoretical value (11.5%) of 6 H_2O molecules per formula of the compound. The large exothermic peak seen in the DTA at ~556 °C corresponds to decomposition of phase II to $Na_4Ge_9O_{20}$ and GeO_2 as confirmed by PXD. The structure of phase II persists up to 556 °C. The DTA–TG curves of phase II are similar to those of phase I except for the absence of the endothermic peak at 160 °C for the former. With increasing temperature, phase II continuously loses two-thirds of its water in the range 50–250 °C and one-third at 250–300 °C without significant endotherms in the latter region. The maximum rate of water loss was observed at 187 and 277 °C, respectively. The total water loss was 6.44% corresponding to four water molecules in the sample.

The transformations indicated by the PXD, DTA and TGA are described by the following reactions:

$$Na_3HGe_7O_{16}{\cdot}6H_2O \rightarrow Na_3HGe_7O_{16}{\cdot}4H_2O + 2H_2O \quad (160\text{–}187\ °C) \quad (3)$$

$$Na_3HGe_7O_{16}{\cdot}4H_2O \rightarrow Na_3HGe_7O_{16} + 4H_2O \quad (187\text{–}220\ °C) \quad (4)$$

$$4Na_3HGe_7O_{16} \rightarrow 3Na_4Ge_9O_{20} + GeO_2 + 2H_2O \quad (>556\ °C) \quad (5)$$

(3) FTIR. The FTIR spectra of three samples, (a) dehydrated $Na_3HGe_7O_{16}$, (b) $Na_3HGe_7O_{16}{\cdot}4H_2O$, and (c) $Na_3HGe_7O_{16}{\cdot}6H_2O$, are shown in Figure 5. The characteristic absorptions of Ge–O asymmetric stretching at 760–765 cm^{-1}, symmetric stretching at ~700 cm^{-1}, and Ge–O–Ge asymmetric stretching at 480–550 cm^{-1} were observed in all samples. Two shoulder bands at 871 and 600 cm^{-1} were seen only in the spectrum of $Na_3HGe_7O_{16}{\cdot}6H_2O$, which indicates the structural difference between $Na_3HGe_7O_{16}{\cdot}6H_2O$ and $Na_3HGe_7O_{16}{\cdot}4H_2O$. For the hydrated samples, phases I and II, the strong H–O–H bending vibration bands at 1622 and 1638 cm^{-1} are evident and the broad hydrogen-bonded O–H stretching bands at 3153–3492 cm^{-1} show the existence of intermolecular hydrogen bonds. The sharp band at 3727–3731 cm^{-1}, which is attributed to the water molecules interacting with the sodium ions,[18] is seen only in the hydrated samples,

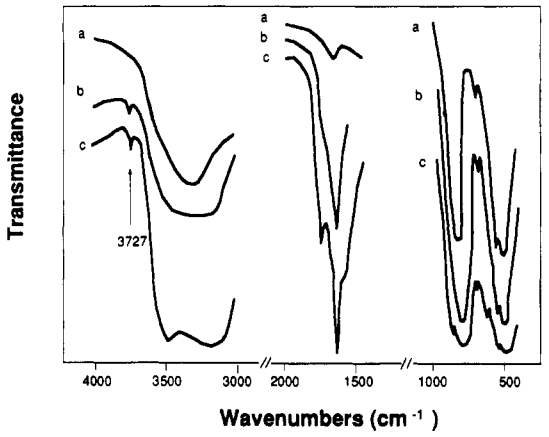

Figure 5. FTIR spectra of (a) dehydrated $Na_3HGe_7O_{16}$, (b) $Na_3HGe_7O_{16}{\cdot}4H_2O$, and (c) $Na_3HGe_7O_{16}{\cdot}6H_2O$.

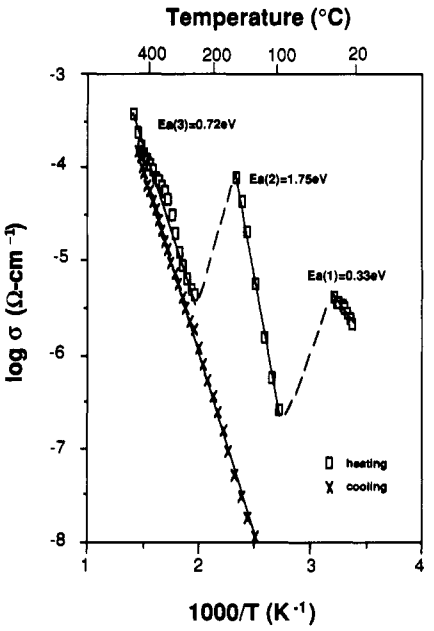

Figure 6. Temperature dependence of conductivity in hydrated $Na_3HGe_7O_{16}{\cdot}6H_2O$.

$Na_3HGe_7O_{16}{\cdot}4H_2O$ and $Na_3HGe_7O_{16}{\cdot}6H_2O$ (Figure 5b,c). For the dehydrated $Na_3HGe_7O_{16}$ this band is not observed; the weak absorption at 1648 and 3392 cm^{-1} is probably due to the adsorption of a small amount of water during the measurement.

Ionic Conductivity in Hydrated Samples. The temperature dependence of conductivity of $Na_3HGe_7O_{16}{\cdot}6H_2O$ from room temperature to ~420 °C shown in Figure 6 exhibits complicated behavior indicative of multiple mechanisms of ionic motion. The conductivity increases from 20 to 50 °C with a relatively small activation energy $E_a(1)$ = 0.33 eV. We ascribed this to be due to the motion of surface protons. Above 50 °C, the surface water is lost and a discontinuity in the conductivity is observed as shown in Figure 7. This is consistent with the DTA-TG data, which show an endotherm and small weight loss (Figure 3 and 7), respectively, in this temperature range. From 94 to 155 °C a large increase [2.7×10^{-7} to 7.8×10^{-5} $(\Omega\ cm)^{-1}$] in the conductivity with an unusually large activation energy $E_a(2)$ = 1.75 eV is seen (Figure 6). The TGA in Figure 3 shows no water loss in this temperature

(18) Ward, J. W. Infrared studies of zeolite surface and surface reactions. In *Zeolite Chemistry and Catalysis*; Rabo, J. A., Ed.; ACS Monograph 171; American Chemical Society: Washington, DC, 1976; 187.

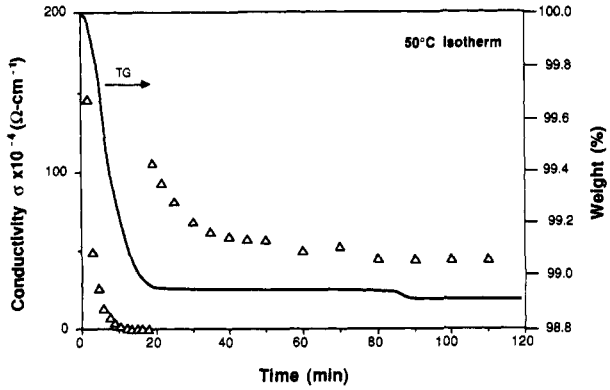

Figure 7. (a) Variation of conductivity with time at 50 °C in $Na_3HGe_7O_{16}·6H_2O$ and (b) TG isotherm curve at 50 °C.

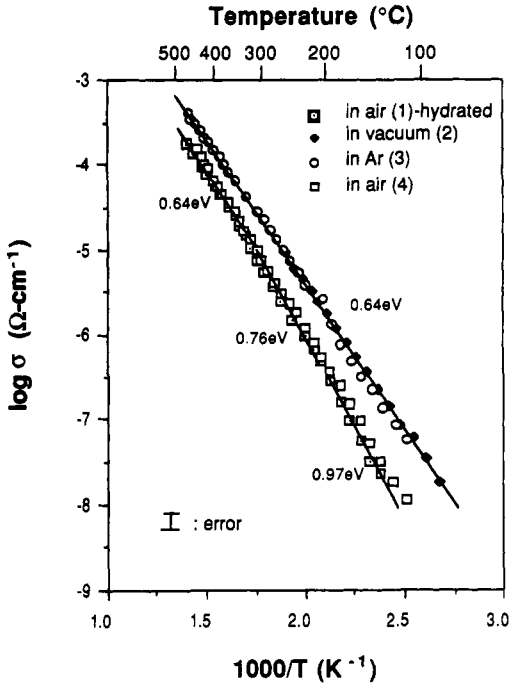

Figure 8. Temperature dependence of conductivity of $Na_3HGe_7O_{16}·4H_2O$ in air (1) and $Na_3HGe_7O_{16}$ in vacuum (2), in Ar (3), and in air (4).

range. The large activation energy implies motion of large $[Na(H_2O)_n]^+$ and/or H_3O^+ ions in the bulk. When the water responsible for the conductivity in this region is lost at about 160 °C (DTA-TG curves, Figure 3), the conductivity decreases. From 246 to 433 °C the conductivity increases again with an activation energy $E_a(3) = 0.72$ eV. Upon cooling the sample, the conductivity follows the heating cycle in the range 433–246 °C and continues to decrease to the lowest measurable value.

Above 160 °C the measurement is made on phase II (i.e., $Na_3HGe_7O_{16}·6H_2O \rightarrow Na_3HGe_7O_{16}·4H_2O$ at 160 °C). Thus the conductivity in this region is best described by Figure 8, curve 1, which depicts the conductivity of $Na_3HGe_7O_{16}·4H_2O$. The temperature dependence of conductivity in air indicates three different linear regions with E_a's: 0.97, 0.76, and 0.64 eV. The observed complicated conductivity mechanism is partly due to the continuous structural change of this phase with water loss and partly to motion of different species in different ranges of temperature. It can be seen that with increasing temperature and decreasing water content in the sample the activation energy decreases.

Sodium Ionic Conductivity in the Dehydrated Sample. To clarify this complicated mechanism of ion

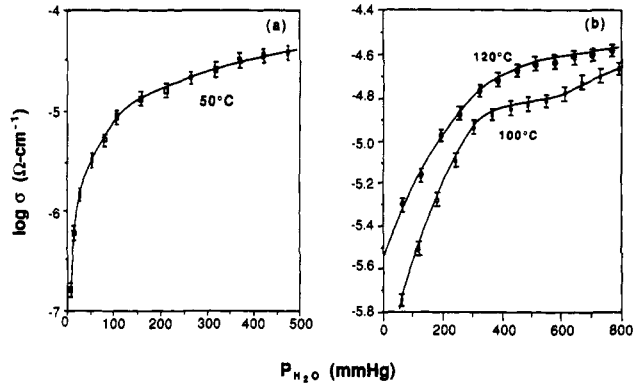

Figure 9. Humidity dependence of conductivity of $Na_3HGe_7O_{16}·6H_2O$ at (a) 50, (b) 100, and 120 °C. Error bars indicate standard deviations.

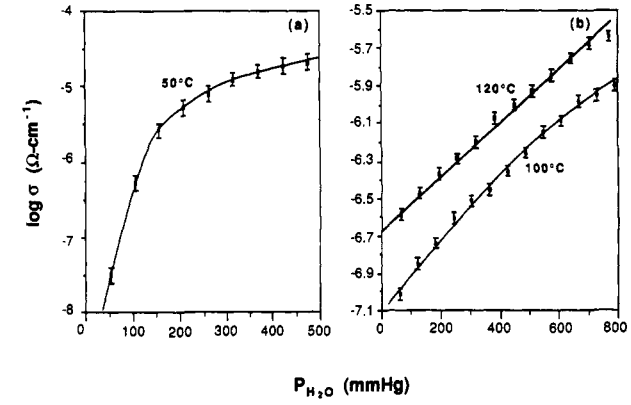

Figure 10. Humidity dependence of conductivity of $Na_3HGe_7O_{16}·4H_2O$ at (a) 50, (b) 100, and 120 °C. Error bars indicate standard deviations.

conductivity in phase II, the conductivity of a dehydrated $Na_3HGe_7O_{16}$ was examined. The Arrhenius plots of conductivity of $Na_3HGe_7O_{16}$ (phase II) in vacuum and in flowing dried Ar gas are linear in the whole temperature range with the same activation energy $E_a = 0.64$ eV (Figure 8, curves 2 and 3). It is noteworthy that the conductivity of the dehydrated sample measured in vacuum or in Ar is higher with a lower activation energy than that of the corresponding dehydrated sample measured in air (i.e., this sample can absorb water from the ambient, Figure 8, curve 4) at the same temperature. For example, at 160 °C the conductivity of the sample in air is 3.2×10^{-8} $(\Omega\ cm)^{-1}$, whereas the same sample in vacuum has a conductivity 3.6×10^{-7} $(\Omega\ cm)^{-1}$. With increasing temperature the four curves (in Figure 8) converge, because at high temperature the dehydrated sample measured in air loses all of its water. This is clear evidence that small amounts of water molecules in the structure can slow down the motion of the sodium ions {i.e., $[Na(H_2O)_x]^+$}. Similar phenomena were observed in other hydrated compounds, such as hydrated β''-alumina.[19] Table I summarizes the conductivities and activation energies in Na-germanates I and II under various conditions.

Humidity-Sensing Property. Although some humidity-sensing materials at room temperature or below 100 °C have been reported,[20-22] few are available for application

(19) (a) Rohrer, G. S.; Farrington, G. C. *Chem. Mater.* **1989**, *1*, 438. (b) Dunn, B.; Farrington, G. C.; Thomas, J. O. *Mater. Res. Soc. Bull.* **1989**, 22.

(20) Yamamoto, T.; Shimizu, H. *IEEE Trans.* **1981**, 149.

(21) Uno, S.; Harata, M.; Hiraki, H.; Sakuma, K.; Yokomizo, Y., *Anal. Chem. Symp. Ser.* **1983**, *17* (Chem. Sens.) 375.

Table I. Conductivities and Activation Energies in Hydrated and Dehydrated Germanates

sample	temp, °C	σ (Ω cm)$^{-1}$	E_a, eV	mobile specie
$Na_3HGe_7O_{16}\cdot 6H_2O$[a] (in air)	23	2.2×10^{-6}	0.33	surface proton
	38	4.1×10^{-6}		
	94	2.7×10^{-7}	1.75	bulk
	155	7.8×10^{-7}		$[Na(H_2O)_x]^+$ and/or H_3O
	246	4.52×10^{-6}	0.72	$[Na(H_2O)_x]^+$
	433	3.84×10^{-4}		
$Na_3HGe_7O_{16}\cdot 4H_2O$ (in air)	147	2.24×10^{-8}	0.97	$[Na(H_2O)_x]^+$
	187	1.60×10^{-7}		
	197	2.82×10^{-7}	0.76	$[Na(H_2O)_x]^+$
	295	7.46×10^{-6}		
	306	1.02×10^{-5}	0.64	Na^+
	444	1.73×10^{-4}		
$Na_3HGe_7O_{16}$ (in Ar)	140	3.25×10^{-8}	0.64	Na^+
	480	8.86×10^{-4}		
$Na_3HGe_7O_{16}$ (in vacuum)	100	1.82×10^{-8}	0.64	Na^+
	253	9.19×10^{-6}		

[a] Above 160 °C the compound is $Na_3HGe_7O_{16}\cdot xH_2O$, x = 0–4 (Na-germanate II).

above 100 °C. The Na-germanates studied here exhibited humidity-sensing properties both below and above 100 °C.

Figures 9 and 10 show the conductivity dependence of $Na_3HGe_7O_{16}\cdot 6H_2O$ and $Na_3HGe_7O_{16}\cdot 4H_2O$ as a function of the partial pressure of water vapor at various temperatures.

For $Na_3HGe_7O_{16}\cdot 6H_2O$ log σ versus P_{H_2O} are similar to those of the adsorption isotherms of typical microporous materials (Figure 9).[1] At 50 °C (Figure 9a) in the low-P_{H_2O} range (<150 mmHg) the conductivity increases rapidly and nearly linearly with humidity, whereas in the high P_{H_2O} range (>400 mmHg) the conductivity increases slowly with increasing P_{H_2O} because the sample is saturated. This is typical of mixed bulk and intergranular (surface) conductivity characteristics. At higher temperature (~100–136 °C), although mixed bulk/surface conductivity behavior is still evident (Figure 9b), the conductivity now is dominated by the surface effects (i.e., S shape of log σ vs P_{H_2O}).

For $Na_3HGe_7O_{16}\cdot 4H_2O$, in the range 50–136 °C, the conductivity is dramatically dependent upon the humidity (P_{H_2O}). At 50 °C the variation of conductivity is about 2.5 orders of magnitude from 5.3×10^{-7} (Ω cm)$^{-1}$ at P_{H_2O} ~ 50 mmHg to 2.1×10^{-5} (Ω cm)$^{-1}$ at P_{H_2O} ~ 450 mmHg. At 136 °C the variation of conductivity is about 0.5 orders of magnitude from 7.0×10^{-7} (Ω cm)$^{-1}$ at ~70 mmHg to 1.8×10^{-6} (Ω cm)$^{-1}$ at ~700 mmHg. For $Na_3HGe_7O_{16}\cdot 4H_2O$ (Figure 10a), the curve of log σ versus P_{H_2O} at 50 °C is S-shaped, whereas above 100 °C the relationship between log σ and P_{H_2O} is nearly linear (Figure 10b). Here, again, as in $Na_3HGe_7O_{16}\cdot 6H_2O$, at low temperature (50 °C) both bulk and intergranular conductivities operate, while at higher temperature (≥100 °C) in the $Na_3HGe_7O_{16}\cdot 4H_2O$ phase the surface conductivity clearly dominates.[23] All humidity-sensing experiments were reversible and reproducible.

The variation of complex impedance of $Na_3HGe_7O_{16}\cdot 4H_2O$ for selected partial pressures of water at 120 °C are presented in Figure 11. Each of the semicircles intersects

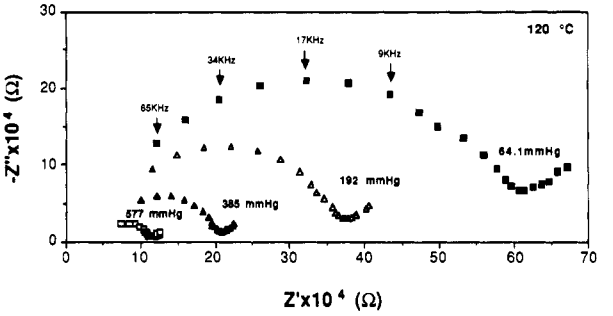

Figure 11. Variation of complex impedance as a function of increasing partial pressure of water, P_{H_2O} at 120 °C.

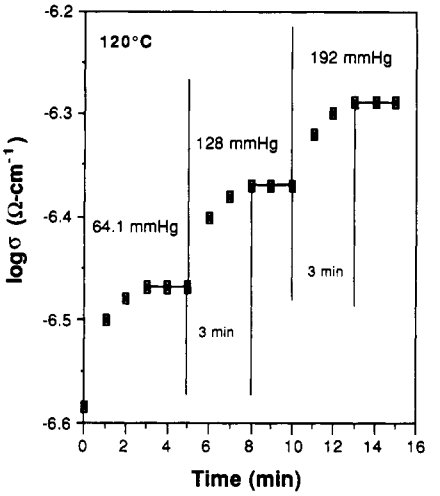

Figure 12. Response time of conductivity to partial pressure of water from 64.1 to 128 mmHg and from 128 to 192 mmHg at 120 °C (note: response time would be significantly better in a flow system; the conditions of the experiment require evacuation followed by introduction of a known amount of H_2O(l) for each new P_{H_2O}; see text).

Z' (at high ω) at the same point, i.e., R_b is not a function of P_{H_2O}. As P_{H_2O} increases, $R_b + R_{ig}$ (i.e., the intersection of the semicircle with Z' at low ω) decreases. This suggests that the conductivity at 120 °C is dominated by the intergranular (or surface) contribution. Ac complex impedance analysis at lower temperature (e.g., 50 °C) indicated that the response of conductivity to humidity was governed by both bulk and intergranular characteristics, i.e., with increasing P_{H_2O} the complex impedance plots clearly showed different values of both R_b and $R_b + R_{ig}$ values.

Figure 12 represents the conductivity response for the $Na_3HGe_7O_{16}\cdot 4H_2O$ with time at various humidities at 120 °C. Before a given "set" humidity can affect the conductivity, the following processes must occur in our static-controlled humidity chamber: (1) phase change of liquid water to gaseous molecular water, $H_2O(l) \rightarrow H_2O(g)$; (2) diffusion of gaseous water molecules to the surface of sample, $H_2O(g) \rightarrow H_2O$(surface of sample); and (3) diffusion of water molecules from surface to bulk of sample, H_2O(surface) $\rightarrow H_2O$(bulk). Thus time for these processes to reach equilibrium is required. In addition, the conductivity response to "set" relative humidity varied for different temperatures and humidities. On the basis of the experimental equilibrium time for conductivity measurement at a given humidity, a safe estimate of conductivity response time is not greater than 3 min.

Proposed Mechanism of Protonation. For the mechanism of protonation on the surface of the germanate particles, we consider the following reaction:

$$Na^+ + n(H_2O)_s = Na(OH)(H_2O)_{n-1} + H^+ \quad (6)$$

(22) Barboux, P.; Morineau, R.; Livage, J. *Solid State Ionics* **1988**, *27*, 221.

(23) Barboux, P.; Livage, J. *Solid State Ionics* **1989**, *34*, 47.

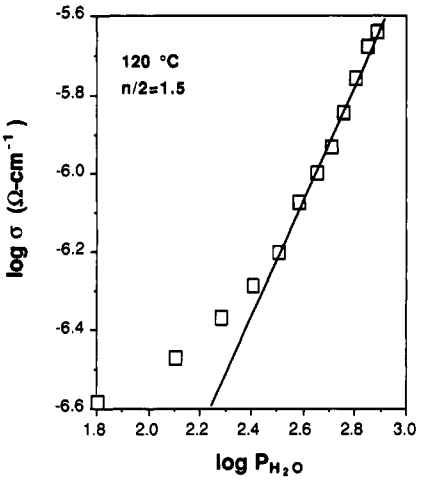

Figure 13. Plot of log σ versus log P_{H_2O} at 120 °C.

where the index s refers to the water on the surface of particle. This mechanism is supported by the presence of ~3720-cm^{-1} peak in the FTIR spectra of hydrated germanates (Figure 5), which was attributed to the interaction of Na^+ with water molecules. The ionization equilibrium can be given as

$$[H^+][Na(OH)\ (H_2O)_{n-1}]/[Na^+][(H_2O)_s]^n = K_0(T) \quad (7)$$

For a small amount of ionization, eq 7 can be written as

$$[H^+] = K_1(T)[(H_2O)_s]^{n/2} \quad (8)$$

Since the conductivity is proportional to the concentration of mobile charge carriers, we have

$$\sigma \propto [H^+] \propto [(H_2O)_s]^{n/2} \propto P_{H_2O}{}^{n/2} \quad (9)$$

To determine the number of water molecules which contribute to the protonation, we plot log σ versus log P_{H_2O} using the conductivity-P_{H_2O} data of phase II at 120 °C (Figure 13). The plot is linear in the range of $P_{H_2O} > 300$ mmHg with a slope of about 1.5. According to Barboux and Livage[23] this indicates that the solvation number (n) of sodium ion on the surface is about 3. This result suggests the motion of protons on the surface of the sample in agreement with the ac impedance analysis, which shows that the conductivity at 120 °C is dominated by the intergranular contribution (Figure 11). Moreover, this result implies that in the temperature range 50–120 °C the mobile species contributing to the conductivity with change of humidity are protons, or H_3O^+ ions, rather then sodium ions associated with water molecules. The solvation number $n > 4.5$ is required for the motion of $Na(H_2O)_n^+$ species.[24,25]

Conclusions

In summary, crystalline microporous $Na_3HGe_7O_{16}\cdot 6H_2O$ was hydrothermally synthesized. In this hydrated compound motion of surface and bulk protons and Na^+ ions respectively dominate the conductivity at different temperatures. Sodium ion conductivity in dehydrated $Na_3HGe_7O_{16}$ (phase II) was observed with conductivities from $\sim 10^{-6}$ $(\Omega\ cm)^{-1}$ at 125 °C to $\sim 10^{-3}$ $(\Omega\ cm)^{-1}$ at 500 °C with E_a = 0.64 eV. Humidity-sensing measurement on the Na–germanates indicated that the conductivity is sensitive to humidity in the temperature range 50–120 °C. The microporous crystalline Na–germanates have potential for application both as sodium conducting electrolytes and humidity-sensing materials.

Acknowledgment. This is publication no. D10550-5-91 of the New Jersey Agricultural Experiment Station supported by State Funds and the Center for Advanced Food Technology (CAFT). The Center for Advanced Food Technology is a New Jersey Commission on Science and Technology Center.

Registry No. $Na_3HGe_7O_{16}\cdot 6H_2O$, 139311-83-4; $Na_3HGe_7O_{16}\cdot 4H_2O$, 12529-63-4; $Na_3HGe_7O_{16}$, 12195-31-2.

(24) Simkovich, G. *J. Phys. Chem.* **1963**, *67*, 1001.
(25) Bockris, J. O'M.; Saluja, P. P. S. *J. Phys. Chem.* **1972**, *76*, 2140.